Journal of Materials Chemistry A

Accepted Manuscript

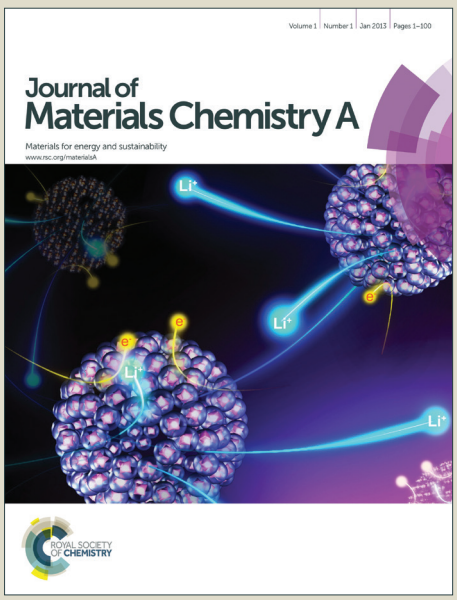

ROYAL SOCIETY OF CHEMISTRY

www.rsc.org/materialsA

Journal of Materials Chemistry A RSCPublishing

Paper

Mesoporous Lithium Vanadium Oxide as Thin Film Electrode for Lithium-Ion Batteries: Comparison between Direct Synthesis of LiV_2O_5 and Electrochemical Lithium Intercalation in V_2O_5

Cite this: DOI: 10.1039/xoxxoooooox

Received ooth January 2014,
Accepted ooth January 2014

DOI: 10.1039/xoxxoooooox

www.rsc.org/

S. Caes,[a] J. C. Arrebola,[a] N. Krins,[a] P. Eloy,[b] E. M. Gaigneaux,[b] C. Henrist,[a] R. Cloots[a] and B. Vertruyen*[a]

Research in the field of lithium-ion batteries favours electrode materials with high surface area. In this context, this paper is dedicated to mesoporous thin films (MTFs) and compares the electrochemical performance of γ-LiV_2O_5 MTFs with post-synthesis electrochemical lithium intercalation in α-V_2O_5 MTFs. Formation of vanadium oxide MTFs by soft-chemistry is notoriously difficult. However, it is shown that wormlike vanadium oxide (V-O) and lithium vanadium oxide (Li-V-O) MTFs can be obtained on silicon substrates by a direct sol-gel soft-templating route (Evaporation Induced Micelles-Packing) using a polystyrene-*block*-poly(ethylene oxide) (PS-*b*-PEO) structuring agent. Heat treatment of 1 minute at 400°C (Li-V-O system) or 30 minutes at 350°C (V-O system) leads to the crystallization of γ-LiV_2O_5 or α-V_2O_5, respectively. These calcination conditions ensure the degradation of the structuring agent while preventing the collapse of the mesostructure, yielding MTFs with pore size diameter in the 30-35 nm range. Using the same set of synthesis conditions, films can be deposited on conductive glass substrates for electrochemical investigation: the α-V_2O_5 films display better specific capacities, while cyclability is good for both compositions, even at a current density as high as 30C-rate.

1. Introduction

Nanomaterials are of great interest in the field of lithium ion batteries because their electrochemical performance at high rates is enhanced thanks to shorter diffusion paths and higher surface area in contact with the electrolyte.[1-4] An illuminating case is that of the lithium vanadium oxide phases. The lithium-free α-V_2O_5 phase has been widely investigated and can be considered as one of the archetypal examples in the field of nanomaterials for electrodes, since it can be prepared with a variety of architectures, such as nanotubes,[5] xerogels,[6] mesoporous powders,[7] or macroporous electrodeposited thin films[8-10] to cite only a few recent publications. However, being a lithium-free positive electrode material, α-V_2O_5 has to be cycled against a metallic lithium negative electrode. This has fueled research on the lithiated phases such as LiV_3O_8 or LiV_2O_5, to be used in lithium-ion batteries. Chemical synthesis of LiV_2O_5 usually yields the γ-LiV_2O_5 phase,[11-14] which differs slightly form the δ-LiV_2O_5 phase obtained by electrochemical intercalation of one lithium in α-V_2O_5.[15] This γ-LiV_2O_5 phase was investigated as a micrometric powder in the early nineties[11] and its performances were found not very promising. It is only quite recently that improved performance at high rate and slightly better specific capacity were reported for nanostructured γ-LiV_2O_5, such as the γ-LiV_2O_5 nanorods studied in 2012 by Wang et al.[13] This suggests that the γ-LiV_2O_5 phase might be worth further investigation.

A recent review paper by Vu et al.[16] has highlighted the advantages of porous electrode materials where pores are defined by a continuous solid framework. In particular, 3D interconnection of the inorganic network at the nanoscale favors good electrical contact and efficient charge transport inside the pore walls. An example of such an architecture is provided by the mesoporous thin films (MTFs) prepared through soft-templating methods combining sol-gel chemistry and block copolymer structuring agents.[17] The successful preparation of MTFs by this synthesis route has been demonstrated for a respectable range of chemical compositions but there have been only a few studies about the preparation of thin film electrodes by this approach. In a previous work,[18] we reported that $NbVO_5$ MTFs displayed higher Li intercalation capacities than the corresponding dense film. In 2011, both

Haetge et al.[19] and Kang et al.[20] reported excellent electrochemical performance at high rates for the anode candidate $Li_4Ti_5O_{12}$ MTFs. These results also represented the first examples of a direct synthesis of lithium - transition metal oxide MTFs by the block copolymer soft-templating route, where 'direct synthesis' means that lithium ions were included in the precursor sol-gel solution, instead of being inserted electrochemically in a pre-existing transition metal oxide MTF.

In order to prepare γ-LiV_2O_5 MTFs, we first tested a direct synthesis route using Pluronic P123 (poly(ethylene oxide)-*block*-poly(propylene oxide)-*block*-poly(ethylene oxide) – EO_{20}-*b*-PO_{70}-*b*-EO_{20}) as a structuring agent.[21] The experimental parameters were such that the templating mechanism was supposed to occur through Evaporation Induced Self Assembly (EISA), i.e., micelles did not pre-exist in the precursor solution but were expected to form in the film due to the increase in P123 concentration driven by solvent evaporation. As reported earlier,[21] we found that MTFs could be obtained for the Li-Ti-O and Li-Nb-O systems but not in the case of the Li-V-O system.

In the present work, we used a PS-*b*-PEO (polystyrene-*block*-poly(ethylene oxide)) structuring agent made up of longer polymeric chains with stronger hydrophilic/hydrophobic contrast than the Pluronics, so that micelles are already present in the precursor solutions. This Evaporation Induced Micelles Assembly (EIMA) process[22] allowed us to obtain both γ-LiV_2O_5 MTFs (section 3.1) and α-V_2O_5 MTFs (section 3.2). Therefore we were able to compare the electrochemical properties of the γ-LiV_2O_5 MTF with the in-situ electrochemical intercalation of lithium in a α-V_2O_5 MTF (section 3.3). Electrochemical cycling of the γ-LiV_2O_5 MTF starts by a charging step (γ-LiV_2O_5 → $V_2O_5 + Li^+ + e^-$) whereas the α-V_2O_5 MTF is first discharged (α-$V_2O_5 + Li^+ + e^-$ → LiV_2O_5).

2. Experimental

2.1 Precursor solutions

The flowchart for preparation of the precursor solutions is as follows. The amphiphilic polystyrene-*block*-poly(ethylene oxide) structuring agent (S_{160}-*b*-EO_{830}, Polymer Source) was dissolved in tetrahydrofuran (THF - For Analysis, ACS, Acros Organics) and heated for a few minutes at 60°C in order to complete solubilisation. Ethanol (analytical reagent grade, Fisher Chemical), lithium chloride (p.a., Merck) and vanadium chloride (VCl_4, 99+%, Acros Organics, 0.9 mol/l in ethanol) were then added to the solution. Finally, distilled water was added in order to induce the hydrolysis of the vanadium species.

The lithium vanadium oxide MTFs were prepared from solutions containing 1.37 10^{-3} mmol PS-*b*-PEO (73.7 mg), 0.67 ml THF, 2.33 ml ethanol, 0.6-0.9-1.35-1.8 mmol LiCl (depending on the desired Li/V molar ratio), 1.8 mmol VCl_4 (2 ml of 0.9 mol l^{-1} VCl_4 in ethanol) and 0.32 ml water.

The vanadium oxide MTFs were prepared from solutions containing 1.85 10^{-3} mmol PS-*b*-PEO (100 mg), 0.52 ml of THF, 1.77 ml of ethanol, 1.8 mmol VCl_4 (2 ml of 0.9 mol l^{-1} VCl_4 in ethanol) and 0.32 ml of distilled water.

2.2 Preparation of MTFs

MTFs of LiV_2O_5 and V_2O_5 were prepared on passivated (001) silicon wafers (Silicium Materials) and FTO-coated glass substrates (60 Ω sq^{-1}, FareTrade, AGC) by dip coating using a 2 mm s^{-1} withdrawal speed in 20% relative humidity. Films were first heated at 200°C for 1 h and finally heated to higher temperature (see results and discussion). Fast heating and cooling rates were achieved by placing and removing the films into/from a pre-heated furnace. All heat treatments were performed in air.

2.3 Characterizations

Precursor solutions were characterized by dynamic light scattering (Viscotek 802 - Omnisize 3.1 software).

Structural and microstructural characterization of films coated on silicon substrates was achieved by a combination of techniques. X-Ray diffraction patterns were collected with a Bruker D8 diffractometer (CuK_α radiation) in grazing incidence configuration with an incident angle of 1°. Transmission electron microscopy (TECNAI G2 TWIN, LaB_6, 200 kV) was performed on fragments of samples scratched from the films. Infra-red spectra were recorded in transmission using a Bruker Equinox 55. Film thickness was determined by ellipsometric spectroscopy performed in the visible spectral range (1.23-3.00 eV) with a SOPRALAB GES-5E instrument. In addition to the optical thickness determination, an atmospheric porosimeter module was used to determine the open porosity and pore size distribution of the films, using toluene as pore filling vapour. More details are given in [21]. X-Ray photoelectron spectroscopy data and spectra are carried out in a Kratos Axis Ultra spectrometer equipped with a monochromatized aluminium X-ray source powered at 10 mA and 15 kV; calibration of the binding energy scale was set by fixing the **C**-(C,H) peak at 284.8 eV; special care was taken to avoid vanadium reduction under vacuum. Grazing Incidence Small Angle X-Ray Scattering was performed at beam line 7.3.3 at the Advanced Light Source, Lawrence Berkeley National Technology, using an X-Ray of 0.123984 nm wavelength. An ADSC Quantum 4R detector was used and the detector distance set at 3.8 meters.

Electrochemical tests were performed using a conventional cell with three electrodes. Two Li foils were used as negative and reference electrodes; the film (deposited on FTO-coated glass substrates and sonicated in THF for 3 minutes) was used as positive electrode. The electrolyte was 1 mol l^{-1} $LiPF_6$ in ethylene carbonate:dimethylcarbonate (1/1:v/v). Cyclic voltammograms and galvanostatic cycles were measured using a PAR 263A potentiostat, from 3.8 V to 2.9 V vs. $Li^+/Li°$. The scan rate of cyclic voltammograms was 0.5 mV s^{-1}. The current densities of galvanostatic cycles were 5.3 µA cm^{-2} (1C-rate) and 160 µA cm^{-2} (30C-rate). As convention, negative current corresponds to the reduction process.

3. Results and Discussion

3.1 Synthesis and (Micro)Structural Characterization of V-O MTFs

As outlined in the introduction, we investigated[21] the direct synthesis of Li-V-O MTFs by EISA in a previous work. The failure to obtain any mesostructure suggests that the presence of lithium ions in the sol-gel precursor solution hindered the micelle formation during the evaporation of the solvent. In the present work, the composition of the precursor solution was therefore modified by replacing the Pluronic structuring agent (P123) with PS-*b*-PEO in order to favour the EIMA mechanism. Characterization of the precursor solution by Dynamic Light Scattering confirmed the presence of micelles, with an average hydrodynamic diameter of ~ 45 nm.

After dip-coating on a silicon substrate, a heat treatment of 1 hour at 200°C was applied to complete the vaporization of the volatile species and promote the condensation of the inorganic Li-V-O oxide network around the micelles formed by the structuring agent. The TEM micrograph in Fig. 1a shows that a wormlike mesostructured film is observed, indicating that the EIMA mechanism is compatible with the presence of lithium ions in the sol-gel precursor solution.

At this stage of the heat treatment, the transmission FT-IR spectrum in Fig. 2a reveals that the PS-*b*-PEO structuring agent is still present in the pores, as shown by the absorption peaks at ~1100 cm^{-1} (PEO) and ~690 cm^{-1} (PS). However, comparison of the FT-IR spectra after 1 hour at 100°C or 200°C suggests a partial degradation of the PEO block at 200°C.

Elimination of the structuring agent is required to transform the hybrid films into MTFs. This is usually achieved by a heat treatment, which plays a triple role: (i) to promote the condensation of the inorganic network, (ii) to induce crystallization of the inorganic network and (iii) to eliminate the structuring agent and free the porosity. The chronology of the three events is influenced by the metal-dependent sol-gel chemistry and the decomposition temperature of the structuring agent. In order to obtain stable MTFs, the condensation of the inorganic network must be sufficiently advanced at the decomposition temperature of the structuring agent so that the inorganic walls possess enough mechanical strength to sustain the elimination of the structuring agent without collapsing. Besides, crystallization is compatible with the MTF structure only if the crystallite size remains equal or smaller than the thickness of the pore walls. An additional requirement in the case of LiV_2O_5 is that vanadium should be present as a mixture of V^{4+} and V^{5+}. Taking into account all these considerations and the results of exploratory tests by X-ray diffraction (Fig. S1 in the ESI†), it was found that the final heat treatment should be short (1 minute) and take place in a pre-heated furnace. In such conditions, LiV_2O_5 is always the first phase to crystallize, whatever the Li/V molar ratio (from 0.33 to 1) whereas extending the duration or increasing the temperature of the heat treatment resulted in the formation of V^{5+} phases (LiV_3O_8, $LiVO_3$).

Fig. 1 shows TEM micrographs and XRD patterns of films prepared from the precursor solution with a Li/V ratio of 0.5 corresponding to the γ-LiV_2O_5 composition. Using 1 minute heat treatments, the mesostructure can be retained up to 400°C (Fig. 1b) while a minimum temperature of 350°C is needed to observe the crystallization of γ-LiV_2O_5 (Fig. 1d). Increasing the temperature to 425°C causes the appearance of a LiV_3O_8 secondary phase (Fig. 1d) and the collapse of the mesostructure (Fig. 1c) due to excessive grain growth of the LiV_2O_5 crystallites (from 27 nm at 400°C to 40 nm at 425°C, as estimated by applying the Scherrer formula to the main XRD reflection).

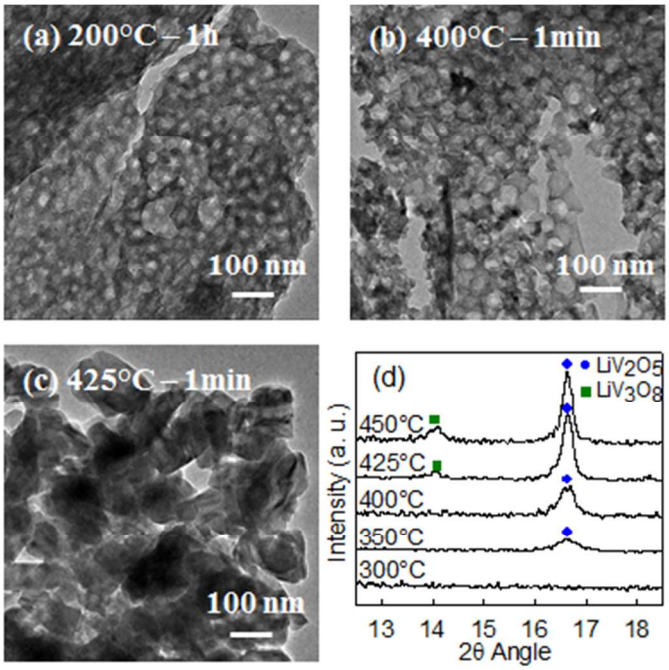

Fig. 1 (a-c) TEM images of Li-V-O thin films heated at different temperatures. (d) X-ray diffractograms of Li-V-O thin films heated for 1 minute at different temperatures.

The shortness (1 minute) of the final heat treatment raises the question of the completeness of the PS-*b*-PEO decomposition needed to transform the hybrid film into a MTF. This means first that the highest temperature compatible with the preservation of the mesoporous structure should be adopted, i.e., 400°C. Transmission FT-IR spectroscopy (Fig. 2a) shows that after 1 minute at 400°C, the characteristic absorption peaks of PS-*b*-PEO are no longer detected. Besides, the atmospheric ellipsometry porosimetry characterization (discussed later in this section) indicates an accessible porosity of 26 %, similar to the value found for $VNbO_5$ MTFs templated by the same PS-*b*-PEO structuring agent but which could be heated to higher temperature (520°C) without collapse of the mesostructure.[23] The decomposition of the PS-*b*-PEO structuring agent in these $VNbO_5$ MTFs was found to be completed by 350°C (10°C/min heating) using thermal ellipsometric analysis.[18] All these results

suggest that the Li-V-O film obtained after 1 minute at 400°C is no longer a hybrid film but indeed a MTF.

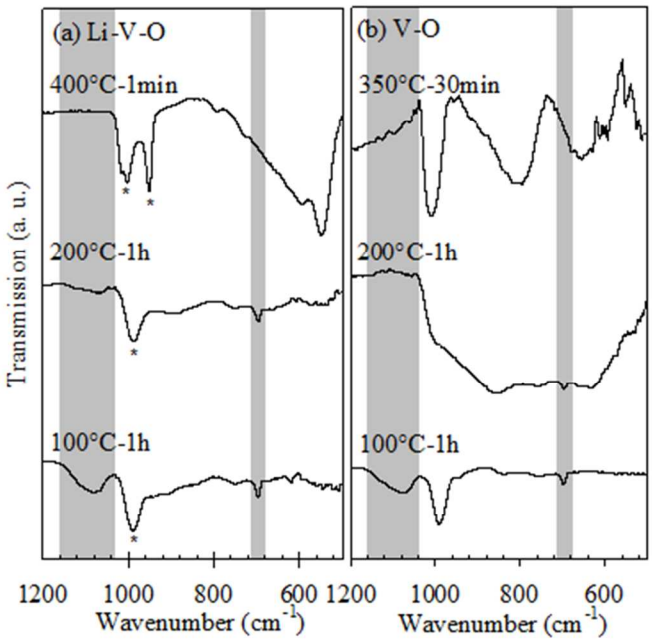

Fig. 2 Transmission IR spectra of (a) Li-V-O thin films and (b) V-O thin films heated at different temperatures. The positions of the absorption bands corresponding to the structuring agent are highlighted in grey. The V=O stretching band of the Li-V-O thin films is marked by asterisks.

The FT-IR spectra mentioned above (Fig. 2a) also provide information regarding the inorganic network: the broad V=O absorption at 1000 cm^{-1} in the amorphous films (at 100°C and 200°C) is replaced by the characteristic absorptions of LiV_2O_5 (V–O–V bending in the 850-500 cm^{-1} range and V=O stretching at 1015 and 942 cm^{-1}) after 1 minute at 400°C. The split-up of the V=O absorption in two peaks is due to the presence of two different bond lengths corresponding to two oxidation states (V^{4+}/V^{5+}).[12] XPS measurements confirm a 55±5 % V^{5+} percentage at the surface of the film (all XPS information is gathered in Fig. S2 and S3 and Table S1 in the ESI†).

In order to analyze its mesoporous structure in more detail, the Li-V-O film heated for 1 minute at 400°C was characterized by atmospheric ellipsometry porosimetry (AEP). The adsorption/desorption isotherm, presented in Fig. 3 (square red symbols), shows a type IV profile (Brunauer classification), which is characteristic of mesoporous materials.[24] An accessible porosity of 26 % was deduced from the adsorbed volume at relative pressure close to 1. The pore size distributions (PSD) derived from the isotherms are shown in the inset of Figure 3. The maximum of the desorption PSD corresponds to the diameter of the pore bottle necks (22 nm), while the pore inside diameter (34 nm) is estimated from the adsorption PSD.[25] Finally, the AEP measurements also give access to the thickness of the film (115 nm).

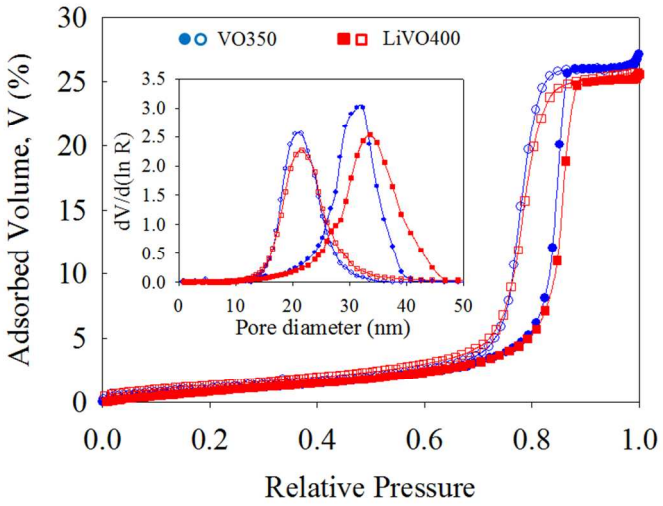

Fig. 3 AEP isotherm curves of a Li-V-O MTF heated at 400°C for 1 minute and a V-O MTF heated at 350°C for 30 minutes (full symbols: adsorption, hollow symbols: desorption). Inset: Corresponding pore size distributions.

The heat treatment at 400°C for 1 minute was also applied to the Li-V-O films deposited on conductive FTO-coated glass substrate in view of electrochemical characterization (cf section 3.3). The modification of substrate does not seem to affect the mesostructure periodicity (see results by Grazing-Incidence Small Angle X-Ray Scattering (GISAXS) in Fig. S4 in the ESI†).

3.2 Synthesis and (Micro)Structural Characterization of V-O MTFs

By comparison with the Li-V-O compositions, the preparation of vanadium oxide MTFs is not complicated by the presence of lithium ions in the precursor solutions. However, the consolidation of the vanadium oxide mesoporous architecture by condensation is difficult due to the presence of V=O bonds which do not participate in the creation of the 3D network and due to the mismatch between the pore curvature and the layered crystalline structure of V_2O_5.[26] The EIMA approach is expected to be more suitable for the preparation of vanadium oxide MTFs, since EIMA structuring agents have a higher decomposition temperature and are able to create larger micelles than the EISA structuring agents tested so far (Brij56/58 – poly(ethylene oxide) hexadecyl ether[26] and P123[21]). Along these lines, we reported in a previous work that PS-*b*-PEO structuring agents can be used to prepare $(V,Nb)_2O_5$ MTFs by EIMA, where the presence of Nb^{5+} helps to stabilize the MTF architecture.[23]

Therefore the PS-*b*-PEO structuring agent used here for the V-O films is the same as for the Li-V-O films in the previous section. The composition of the sol-gel precursor solution reported in the experimental section for the preparation of vanadium oxide MTFs has been adapted from our earlier work on $(V,Nb)_2O_5$,[23] mainly by reducing the THF content to favour larger micelles. After dip-coating on a silicon substrate and heat

treatment at 200°C for 1 hour, a wormlike mesostructured film is obtained as seen in Fig. 4a. The FT-IR spectrum of this hybrid film (Fig. 2b, 200ºC-1h) reveals only the presence of the characteristic absorption of the polystyrene block. This faster decomposition of PEO in the lithium-free vanadium oxide films confirms our previous observations.[21]

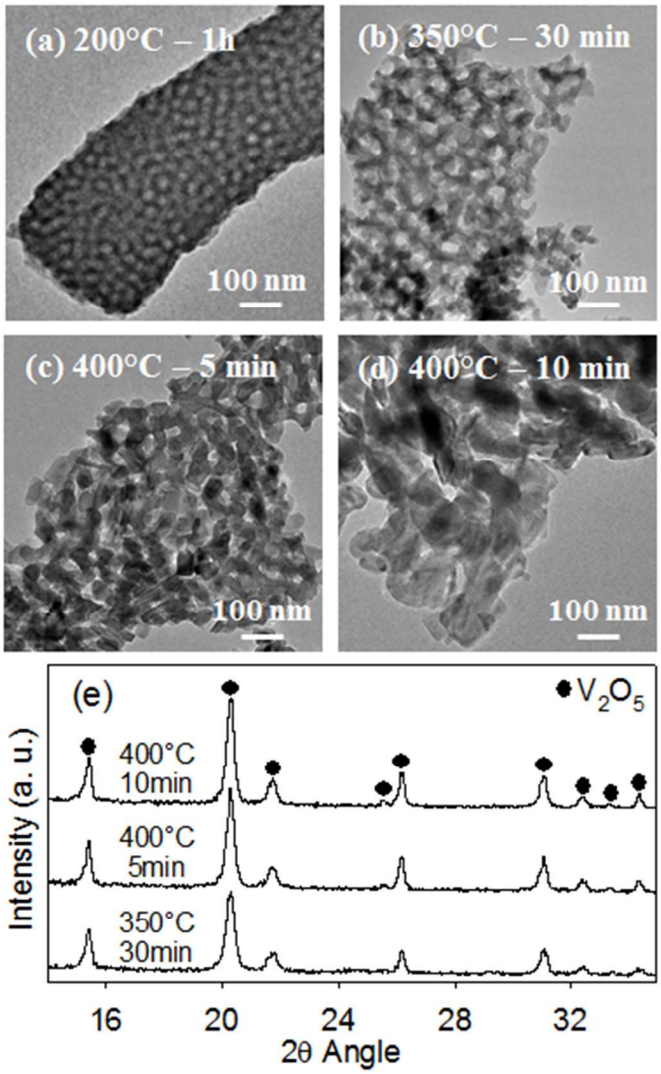

Fig. 4 (a-d) TEM images of V-O thin films heated at different temperatures. (e) X-ray diffractograms of V-O thin films heated at different temperatures.

The calcination conditions were adjusted by progressively reducing the temperature with respect to the heat treatment used for the $NbVO_5$ system,[23] in order to account for the lower crystallization temperature of the niobium-free vanadium oxide. Fig. 4 shows TEM micrographs and XRD patterns of films heated to 400°C or 350°C for various durations. In all cases the reflections in the XRD patterns correspond to α-V_2O_5 (Fig. 4e). Heating at 400°C for 10 or 5 minutes causes a complete or partial collapse of the mesostructure, respectively (Fig. 4c and d). Therefore the calcination temperature was decreased to 350°C, while the duration of the heat treatment was increased to ensure decomposition of the structuring agent (see FT-IR spectra in Fig. 2b, 350ºC-30min). There was no risk of excessive oxidation of the vanadium in the present case since the desired V_2O_5 phase contains only V^{5+}. A heat treatment of 30 minutes at 350°C allowed us to obtain a wormlike MTF (Fig. 4b) with α-V_2O_5 crystalline phase (Fig. 4e). XPS measurements on the film surface confirm that vanadium is found exclusively as V^{5+}.

The AEP profile of the V-O MTF heated at 350°C for 30 minutes is shown in Fig. 3 (circle blue symbols) and is very similar to that of the Li-V-O MTF heated at 400°C for 1 minute, with similar pore size (32 nm vs. 34 nm for the inside pore diameter and 22 nm in both cases for the bottle neck diameter). The vanadium oxide film is slightly thicker (135 nm instead of 115 nm). However, when the V-O film is deposited on conductive FTO-coated glass substrate in view of electrochemical characterization, the modification of substrate appears to affect the grain growth and results in significantly different microstructures: scanning electron micrographs (Fig. S5 in the ESI†) of the film surfaces shows that aggregates of elongated grains (film on FTO-coated glass) are obtained instead of the continuous wormlike network (film on Si).

3.3 Synthesis and (Micro)Structural Characterization of V-O MTFs

Cyclic voltammetry and galvanostatic charge/discharge cycling were used to characterize the electrochemical performance of the Li-V-O and V-O films, deposited on FTO-coated glass substrates using the synthesis conditions discussed above (400°C/1 min, called *LVO400* and 350°C/30 min, called *VO350*, respectively). Fig. 5 displays the cyclic voltammograms at 0.5 mV/s and the 1st and 30th galvanostatic cycles at 1C-rate, between 2.9 V and 3.8 V vs. $Li^+/Li°$. As an additional contribution to the discussion, ex-situ XRD patterns (Fig. 6) were recorded before cycling, at full (dis)charge and after 1 complete cycle at 1C-rate. The main reflections of the underlying FTO layer are visible in all patterns.

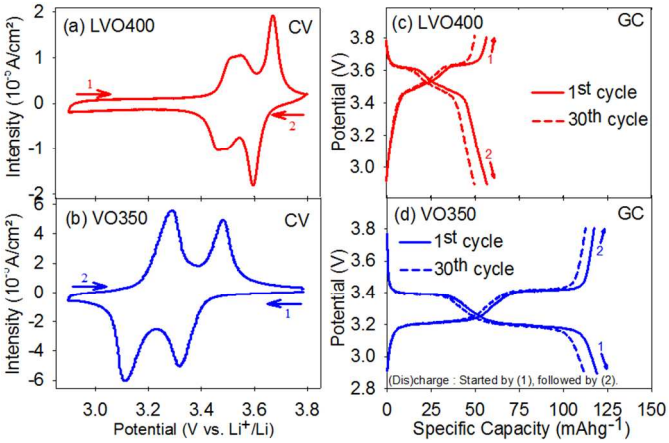

Fig. 5 *LVO400* and *VO350* films. (a,b) Cyclic voltammograms at 0.5mV/s and (c,d) 1C-rate galvanostatic charge/discharge curves of the 1st and 30th cycle between 2.9 V and 3.8V.

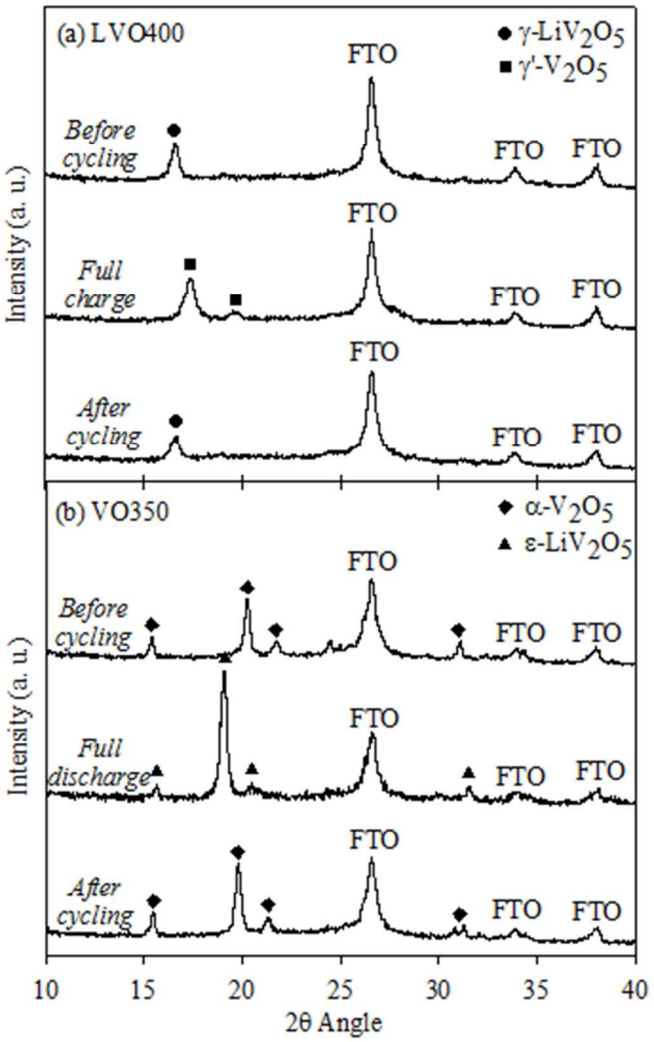

Fig. 6 XRD diffractograms of (a) *LVO400* film and (b) *VO350* film at different stage of the electrochemical cycling.

In the case of the *LVO400* voltammogram (Fig. 5a), the oxidation (charge) of γ-LiV_2O_5 proceeds through two steps: a broad peak at 3.55 V and a sharp peak at 3.7 V. Corresponding plateaus are seen in the galvanostatic curves (Fig. 5c). The XRD pattern of the film after charge to 3.8 V corresponds to the γ'-V_2O_5 phase (Fig. 6a, 'full charge'), as expected from the results of Cocciantelli et al.[27] Reduction (discharge) of the γ'-V_2O_5 phase regenerates the γ-LiV_2O_5 phase (Fig. 6a, 'after cycling'). The XRD and the shape of the CV and galvanostatic curves are coherent with the (des)intercalation of one equivalent of Li^+ in the film. However, the 57 $mAhg^{-1}$ capacity (Fig. 5c) represents only 39 % of the theoretical capacity and is indeed much lower than the 130 $mAhg^{-1}$ obtained by Barker et al.[14] On the other hand, the XRD pattern shows a complete conversion of the crystalline γ-LiV_2O_5 into γ'-V_2O_5. A possible explanation could be that only the topmost layer of the film is crystallized and accessible after the 1-minute heat treatment at 400°C. By comparison with the Si-substrate, the FTO-coated glass substrate is 1.7 times thicker and the thermal conductivity of glass is approx. 100 times lower than that of silicon.[28] Therefore, the FTO-coated glass substrate reaches a lower temperature before the removal of the sample from the pre-heated furnace after 1 minute. This hypothesis is supported by the fact that the crystallite size is lower in the film deposited on FTO-coated glass (20 nm instead of 27 nm). Attempts to increase the duration of the heat treatment resulted in collapse of the porosity and crystallization of LiV_3O_8 instead of γ-LiV_2O_5, without improvement of the capacity.

The *VO350* film exhibits the expected electrochemical behavior in discharge, with two peaks in the cyclic voltammogram (Fig. 5b) and the corresponding plateaus in the galvanostatic curve (Fig. 5d).[29-31] The XRD pattern obtained after discharge to 2.9 V (Fig. 6b, 'full discharge') shows the reflections of the ε-$Li_xV_2O_5$ phase, reported to exist for x up to ~ 0.85.[15] This is coherent with the capacity value of 120 $mAhg^{-1}$, which corresponds to 81% of the theoretical value calculated for insertion of 1 Li^+ per V_2O_5. A similar behavior has been reported for V_2O_5 films by other authors.[30,32] Oxidation (charge) of the ε-LiV_2O_5 phase does not perfectly regenerate the initial α-V_2O_5 phase (Fig. 5b, 'after cycling'), since there is a shift of the (001) reflection from 2θ = 20.28° to 19.80°. This corresponds to an increase in the distance between the V_2O_5 layers after cycling, probably due to some irreversibly intercalated lithium.

Since the motivation of using porous materials for electrodes is that they should perform well at high rates, the capacity retention of the *LVO400* and *VO350* films was investigated both at medium (1C-rate) and high (30C-rate) rates, as shown in Fig. 5 and 7. Charges and discharges were carried out at the same rate (either 1C or 30C). After 30 cycles at 1C-rate, the *LVO400* and *VO350* films retain 88 % and 95 % of their initial capacity, respectively, with coulombic efficiencies of 99.5% or more after the first few cycles (Fig. 7a). In the case of cycling at 30C-rate (Fig. 7b), several cycles are necessary before reaching the maximum capacity values, only 25-33% lower than the 1C-rate values thanks to the porous architecture. The retention after 100 cycles at 30C-rate is very good in the case of the *VO350* film while the capacity of the *LVO400* film decreases again after ~75 cycles. Regarding the film microstructures, cycling at 1C or 30C does not cause microstructural reorganization (Fig. S6 in the ESI†).

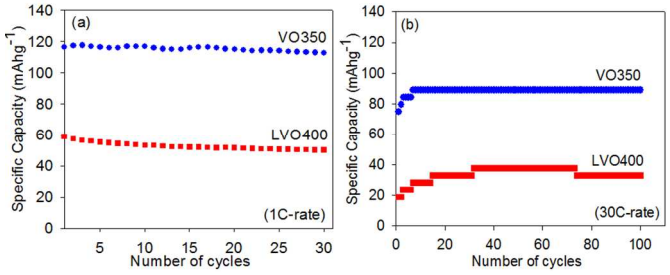

Fig. 7 Specific capacity for (a) the first 30 cycles at 1C-rate and (b) the first 100 cycles at 30C-rate of *VO350* and *LVO400*.

4. Conclusions

Considering that the mesoporous thin film architecture offers high surface area and short diffusion distances, this work investigated the possibility to prepare lithium vanadium oxide and vanadium oxide mesoporous thin films (MTFs) by the direct sol-gel evaporation-induced micelle packing assembly (EIMA) method using PS-*b*-PEO as surfactant. Using silicon substrates, γ-LiV_2O_5 and α-V_2O_5 wormlike MTFs were obtained after heat treatment of 1 minute at 400°C or 30 minutes at 350°C, respectively. The degradation of the structuring agent was confirmed by infrared spectroscopy and the pore diameter reaches 30-35 nm for both films.

In order to compare the electrochemical performances of the γ-LiV_2O_5 MTFs (where lithium ions are present in the structure at the synthesis stage) with the electrochemical intercalation of lithium ions in α-V_2O_5 MTFs, films were deposited on conductive glass substrates, using the same set of synthesis conditions. The crystalline phase transformations during the charge and discharge process were followed by ex-situ XRD, with γ-LiV_2O_5 yielding γ'-V_2O_5 on lithium deintercalation and α-V_2O_5 transforming into ε-LiV_2O_5 on lithium intercalation. Galvanostatic cycles performed at 1C-rate showed a better specific capacity for α-V_2O_5 MTFs (81 % of the theoretical value), compared to γ-LiV_2O_5 films. In both cases, the capacity decreased by only 25-30% when increasing the cycling rate from 1C to 30C. Both films present a coulombic efficiency higher than 99%, with a good cyclability even at 30C-rate especially for the α-V_2O_5 MTFs.

More generally, this work confirmed that the γ-LiV_2O_5 phase, when nanostructured, is able of reversible cycling. This is an interesting point since γ-LiV_2O_5 is the lithiated form of the positive electrode material, contrary to α-V_2O_5 that requires a metallic lithium negative electrode as a source of lithium. Besides, the successful preparation of a γ-LiV_2O_5 MTF by the EIMA approach demonstrates that using structuring agent that form micelles in the precursor solution is a promising strategy to expand the range of MTF compositions with poor network-forming abilities such as lithium ions. However, there is a need for further work to try to identify systematic rules for the optimization of the heat treatment in order to control the decomposition of the structuring agent and the crystallization while retaining the mesostructure.

Acknowledgments

Part of this work was supported by the Belgian Science Policy (Belgian State) under the Interuniversity Attraction Poles program (INANOMAT-P6/17). N.K. thanks the F.R.S.-FNRS (National Fund for Scientific Research) in Belgium for a research fellowship. NK is grateful to Prof. D. Milliron and Advanced Light Source (Lawrence Berkeley National Laboratory, Berkeley, USA) for access to beamline 7.3.3. The authors thank Alexis Bourgeois for AEP analysis.

Notes and references

[a] LCIS/GREEn-Mat, Department of Chemistry, Chemistry Institute B6, University of Liège, 4000 Liège, Belgium.
[b] Institute of Condensed Matter and Nanosciences (IMCN), Division "MOlecules, Solids and reactiviTy" (MOST), Université catholique de Louvain, 1348 Louvain-la-Neuve, Belgium.

† Electronic Supplementary Information (ESI) available: XRD summary of crystalline phases obtained for different Li/V molar ratio in function of the temperature, XPS data and spectra of V-O and Li-V-O films, a GISAXS comparison of V-O and Li-V-O films deposited on silicon and FTO-Glass substrates, SEM images of the surface of V-O and Li-V-O films deposited on silicon and FTO-Glass substrates and after electrochemical cycling. See DOI: 10.1039/b000000x/

1 C. N. Chervin, J. W. Long, N. L. Brandell, J. M. Wallace, N. W. Kucko and D. R. Rolison, *J. Power Sources*, 2012, **207**, 191.
2 V. Augustyn and B. Dunn, *Electrochimica Acta*, 2013, **88**, 530.
3 D. A. Tompsett, S. C. Parker, P. G. Bruce and M. S. Islam, *Chem. Mater.*, 2013, **25**, 536.
4 J. C. Arrebola, A. Caballero, M. Cruz, L. Hernán, J. Morales and E. R. Castellón, *Adv. Funct. Mater.*, 2006, **16**, 1904.
5 X. Zhou, G. Wu, G. Gao, J. Wang, H. Yang, J. Wu, J. Shen, B. Zhou and Z. Zhang, *J. Phys. Chem. C*, 2012, **116**, 21685.
6 D. Liu, Y. Liu, A. Pan, K. P. Nagle, G. T. Seidler, Y.-H. Jeong and G. Cao, *J. Phys. Chem. C*, 2011, **115**, 4959.
7 S. B. Bukallah, A. Bumajdad, K. M. S. Khalil and M. I. Zaki, *Appl. Surf. Sci.*, 2010, **256**, 6179.
8 S. Wang, S. Li, Y. Sun, X. Feng and C. Chen, *Energy Environ. Sci.*, 2011, **4**, 2854.
9 S. R. Li, S. Y. Ge, Y. Qiao, Y. M. Chen, X. Y. Feng, J. F. Zhu and C. H. Chen, *Electrochim. Acta*, 2012, **64**, 81.
10 Y. Liu, J. Li, Q. Zhang, N. Zhou, E. Uchaker and G. Cao, *Electrochem. Commun.*, 2011, **13**, 1276.
11 J. M. Cocciantelli, M. Ménétrier, C. Delmas, J. P. Doumerc, M. Pouchard and P. Hagenmuller, *Solid State Ionics*, 1992, **50**, 99.
12 A. M. El-Sayed and S. M. A. Mousa, *J. Chin. Chem. Soc.*, 2006, **53**, 559.
13 W. Wang, H. Wang, S. Liu and J. Huang, *J. Solid State Electrochem.*, 2012, **16**, 2555.
14 J. Barker, M. Y. Saidi and J. L. Swoyer, *J. Electrochem. Soc.*, 2003, **150**, A1267.
15 C. Delmas, H. Cognac-Auradou, J. M. Cocciantelli, M. Ménétrier and J. P. Doumerc, *Solid State Ionics*, 1994, **69**, 257.
16 A. Vu, Y. Qian and A. Stein, *Adv. Energy Mater.*, 2012, **2**, 1056.
17 P. Innocenzi and L. Malfatti, *Chem. Soc. Rev.*, 2013, **42**, 4198.
18 N. Krins, J. D. Bass, D. Grosso, C. Henrist, R. Delaigle, E. M. Gaigneaux, R. Cloots, B. Vertruyen and C. Sanchez, *Chem. Mater.*, 2011, **23**, 4124.
19 J. Haetge, P. Hartmann, K. Brezesinski, J. Janek and T. Brezesinski, *Chem. Mater.*, 2011, **23**, 4384.
20 E. Kang , Y. S. Jung , G. H. Kim , J. Chun , U. Wiesner, A. C. Dillon, J. K. Kim and J. Lee, *Adv. Funct. Mater.*, 2011, **21**, 4349.
21 S. Caes, C. Malherbe, N. Krins, J. C. Arrebola, C. Henrist, R. Cloots and B. Vertruyen, *Micropor. Mesopor. Mat.*, 2013, **172**, 87.
22 C. Sassoye, C. Laberty, H. L. Khanh, S. Cassaignon, C. Boissière, M. Antonietti and C. Sanchez, *Adv. Funct. Mater.*, 2009, **19**, 1922.
23 N. Krins, L. Lepot, R. Cloots and B. Vertruyen, *Solid State Ionics*, 2009, **180**, 848.

24 S. Brunauer, L. Deming, W. Deming and E. Teller, *J. Am. Chem. Soc.*, 1940, **62**, 1723.
25 M. Etienne, A. Quach, D. Grosso, L. Nicole, C. Sanchez and A. Walcarius, *Chem. Mater.*, 2007, **19**, 844.
26 E. L. Crepaldi, D. Grosso, G. J. de A. A. Soler-Illia, P.-A. Albouy, H. Amenitsch and C. Sanchez, *Chem. Mater.*, 2002, **14**, 3316.
27 J. M. Cocciantelli, P. Gravereau, J. P. Doumerc, M. Pouchard and P. Hagenmuller, *J. Solid State Chem.*, 1991, **93**, 497.
28 CRC Handbook of Chemistry and Physics, 84th Edition, CRC Press, 2003-2004.
29 J. Swiatowska-Mrowiecka, V. Maurice, S. Zanna, L. Klein and P. Marcus, *Electrochim. Acta*, 2007, **52**, 5644.
30 E. A. Meulenkamp, W. van Klinken and A. R. Schlatmann, *Solid State Ionics*, 1999, **126**, 235.
31 I. Quinzeni, S. Ferrari, E. Quartarone and P. Mustarelli, *J. Power Sources*, 2011, **196**, 10228.
32 R. Baddour-Hadjean, J. P. Pereira-Ramos, C. Navone and S. Smirnov, *Chem. Mater.*, 2008, **20**, 1916.